

Role of non-classical paths of a photon in the density of optical states

Kritika Jain and Murugesan Venkatapathi*

Computational and Statistical Physics Laboratory, Indian Institute of Science, Bangalore, 560012

The modified density of optical states due to a weak coupling with external cavities or other resonant objects (Purcell effect), can be recast as a quantum interference of the classical paths of the photon that effect the scattering and absorption by the object. When the coupling is stronger, additional paths representing the (Rabi oscillations or) possible re-absorption of the photon from the excited object, by the emitter at ground-state, have to be included in the quantum interference. The effect of these additional non-classical paths of the photon on the efficiency of spontaneous emission, can be included using a simple one-loop correction to the weak-coupling approximation. This effect is especially evident in the anomalous enhancements of emission due to extremely small fully absorbing metal nanoparticles less than 10 nm in dimensions. Extending these corrections to a collective model of spontaneous emission that includes multiple emitters and such very small metal nanoparticles coupled to each other, the large contribution of non-classical paths to radiative decay in such bulk materials is elucidated.

I. INTRODUCTION

The role of vacuum modes on spontaneous emission of photons has been well elucidated and the reversible exchange of a photon between a mode of vacuum and an atom inside a micro-cavity is observable [1–4]. This Rabi oscillation of the excitation between the cavity and a resonant atom is the sign of a strongly coupled atom-vacuum system, and the coupling strength inferred by the ratio of the frequency of oscillation and the decay rate of the cavity is large ($\Omega/\Gamma > 1$). In the absence of the cavity i.e. weak coupling of the emitter with vacuum, when a proximal resonant object is introduced, such Rabi oscillations with the object can emerge indicating a strong coupling with it [5–7]. The increase in decay rates due to the presence of the proximal object, is given by the additional modes available for the spontaneous emission [8].

Even in this case of a strong coupling, the partition of optical states into the radiative and non-radiative parts reflected the classical absorption and scattering properties of this object [9–12]. It was shown that the conventional partition can result in significant anomalies when the emitter is strongly coupled to absorbing matter [13, 14]. This anomaly is also related to the large unexpected gains of emission in surface-enhanced-Raman-spectroscopy (SERS) where a strongly absorbing resonant metal structure increases the radiation exciting a molecule in the near-field by orders of magnitude, but surprisingly without apparent absorption of the emitted photons. This divergence of SERS from first principle theoretical models has increased during which the reported SERS enhancements have grown from 10^4 to 10^{14} [15–18]. Further, anomalous enhancements of spontaneous emission near fully absorbing metal nanoparticles less than 10 nm in dimensions, have been reported [19–22].

We begin with a phenomenological description of the strong-coupling regime of the emitter and a nanostructure, to deduce a simple correction to the conventional partition of optical states into radiative and non-radiative parts. This renormalization of the radiative and non-radiative parts invokes the emitter’s possible re-absorption of the photon from the excited dissipating structure, to include an one-loop correction [13]. It can be equally described as the result of non-Markovian interaction between the emitter and the proximal absorbing object, where the decay from the emitter and the object are not two independent processes. The effects of non-Markovian interactions on the total decay, and its dynamics, have been studied before [23–25]. A first principles model of the effect of non-Markovian interaction between an emitter and a metal nanoparticle, on the radiative and non-radiative parts of the decay, validates this one-loop correction [26]. The one-loop correction for the efficiency of emission is especially useful for studying bulk materials with many emitters and the smaller metal nanostructures interacting with each other, and is the main goal of this work. In this paper, we extend this correction of the radiative and non-radiative decays to a collective model of many coupled emitters and metal particles, and use it to study this effect in such materials.

One can recast the modified spontaneous emission due to a body as a quantum interference of all the possible paths of the emitted photon [27–29]. The resulting effects on the radiative and non-radiative decay channels can be explained succinctly using figure 1. When we include the non-classical paths of the photon, which include the re-absorption of a photon by the emitter that would have otherwise dissipated in the object, it permits a fully absorbing non-scattering object to increase the efficiency of spontaneous emission. Note that these closed loops of the photon between the emitter and object are inconsequential in classical optics.

When the frequency of Rabi oscillations with the object is significantly less than the decay rate of the emitter in free-space i.e. $\Omega \ll \Gamma_o$, the interaction is incoherent and the emitter is uncoupled, and we observe no effect

* muruges@iisc.ac.in

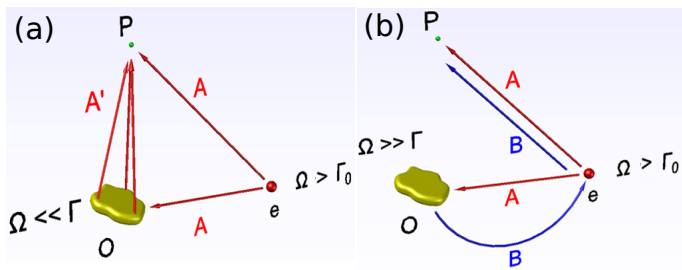


FIG. 1. Coupling of emitter e with object O and resulting coherent paths of the photon to a point P ; Ω is the frequency of emitter-object Rabi oscillations, Γ and Γ_o are the decay rates from the object and the emitter in free-space respectively (a) Interference of direct path A with classical paths A' represents additional decay due to the object (b) Interference of path A with non-classical path B (in blue) represents a coherent decay of the emitter and object.

of the object on the emission. When the resonant object is relatively close to the emitter, the increase in coupling strength with $\Omega \sim \Gamma_o$, renders the classical paths AA' through the object and the direct free-space path A shown in figure 1a, indistinguishable. But note that this path A' is dominant only when the decay from the object is significantly faster than the Rabi oscillations ($\Gamma \gg \Omega$). The above condition signifies the weak coupling of the emitter with the object. It is known that the interference of these two paths A and A' at all points P , given by the superposition of the scattered field from the object and the direct field from the emitter, provides us the additional radiative and non-radiative decay due to the object [30].

However, when the emitter is strongly coupled to the object ($\Gamma \ll \Omega$) and we consider only a single Rabi oscillation, paths A' become irrelevant as Rabi oscillations are much faster than the decay in the object. The dominant path of the photon through the object is now path B , and its interference with A as shown in figure 1b should be of primary interest. The crucial difference in this path is that there is no decay in the object and hence no absorption. In case the probabilities of both these paths are comparable ($\Gamma \sim \Omega$), the two cases of interference (1a and 1b) can be averaged with the corresponding probabilities of these mutually exclusive paths given by $1 - e^{-\frac{\Gamma}{\Omega}}$ and $e^{-\frac{\Gamma}{\Omega}}$.

The decay rates Γ^r and Γ^{nr} of a metallic object evaluated using only paths A' have to be renormalized to evaluate the actual quantum efficiencies of emission. Let Γ_o^r and Γ_o^{nr} be the known radiative and non-radiative decay rates of the isolated emitter adding to Γ_o . Γ^r and Γ^{nr} add to the total metallic contribution Γ , and the total radiative and non-radiative rates of the system are a sum of the free-space and metallic components. The coherent decay of the emitter and object through path B , where dissipation is absent, carries more significance for the dipole mode of the object that represents its coupling to vacuum modes. The substitution of the paths

A' with path B , replaces non-radiative decay of the object's dipole mode numbered '1' with radiative decay [13]. Using the probability of this path B given by $e^{-\frac{\Gamma}{\Omega}}$, the renormalized partition of decay rates is given by:

$$\Gamma_{leak} = e^{-\frac{\Gamma}{\Omega}} \cdot \Gamma_1^{nr} \quad (1)$$

The effective decay rates are:

$$\Gamma_{eff}^r = \Gamma_o^r + \Gamma^r + \Gamma_{leak} \quad (2)$$

$$\Gamma_{eff}^{nr} = \Gamma_o^{nr} + \Gamma^{nr} - \Gamma_{leak} \quad (3)$$

The non-classical paths also make the dynamics of emission non-Markovian i.e. exponentially damped oscillatory decay for a single excitation, which can manifest as a multi-exponential decay in ensembles [24, 25]. Since the one-loop correction is directed at the weak to moderate coupling strengths as in our examples, and we are interested in the time-averaged quantities, we ignore these marginal effects.

II. METHODS

The significant question of interest here is if this coherence of non-classical paths survive when multiple emitters are strongly coupled to metal nanoparticles. This is practically significant as bulk materials have many emitters, and even single emitters like quantum dots have a size-effect on the strength of coupling [14]. Of specific interest are the extremely small metal nanoparticles which have a negligible scattering efficiency and are fully absorbing; see the appendix for the variation of the strength of coupling with size of metal nanoparticles. In the rest of this paper we use a model of many coupled dipole emitters and metal particles, both with and without including the non-classical paths described above, to elucidate the density of optical states in such materials.

A coupled system of Lorentz dipole oscillators was used to model an excitation of one quantum of energy shared among identical emitters. It represents weak excitations given by one excited emitter among the N possible emitters i.e. superpositions of one excited emitter and $N - 1$ other emitters at ground state [31–33]. The coupling of this ensemble of emitters with a metal particle (Figure 2a) as required for the study here, is included by the modification of the Green tensors coupling the emitters due to the addition of the nanoparticle. This model was first treated analytically under long-wavelength approximations for a spherical metal particle [34], was extended to retarded waves [10], and also to arbitrary geometries without long-wavelength approximations [35]. The pairwise self-energy contribution of N coupled Lorentz dipole oscillators proximal to metal nanostructure is:

$$\Sigma_{jk}^{total}(\omega) = \frac{-2\pi q^2 \omega}{mc^2} \mathbf{e}_j \cdot \mathbf{G}(\mathbf{r}_j, \mathbf{r}_k; \omega) \cdot \mathbf{e}_k - \delta_{jk} \frac{i\Gamma_o}{2} \quad (4)$$

$$= \Delta_{jk}^{total} - \frac{i\Gamma_{jk}^{total}}{2} \quad (5)$$

and the above can be integrated over polarization vectors \mathbf{e} , and with a line-shape around the emission frequency ω_0 if required. Here q is the oscillating charge, m is its mass, and c is speed of light. The decay rate is given by the imaginary part where the reduced Planck's constant was divided out of the self-energy in equation(4). This model represents a dipole approximation of a two-level emitter in the weak vacuum-coupling regime, and it uses the Fermi golden rule to relate the decay rates to the density of optical states [36, 37].

This widely used conventional description of the self-interaction in equation (4) includes an implicit rotating wave approximation ($|\Re(\Sigma)| \ll \omega$). The real part of self-energy represents the coupling strength g and also energy split ΔE between the two modes of the strongly coupled oscillators [34, 38]:

$$\Omega = 2g = 2|\Re(\Sigma)| = \frac{\Delta E}{\hbar} \quad (6)$$

where \hbar is the reduced Planck's constant. The above Rabi frequency Ω can be further generalized to include the effects of dephasing due to asymmetry in the damping of the two oscillators [12, 39–41].

Δ_{jk}^{total} and Γ_{jk}^{total} represent entries of $N \times N$ matrices. Each component of matrix $\Delta_{jk} = \Re(\Sigma_{jk}^{total})$ represents the virtual photon exchange between two dipoles at position \mathbf{r}_j and \mathbf{r}_k in presence of metal nanostructure and matrix $\Gamma_{jk} = -2\Im(\Sigma_{jk})$ represents effects of the coupling on decay rates of the two dipole emitters. Green dyadic \mathbf{G} represents interaction between the two dipole emitters in the presence of the metal nanostructure. The self-energy matrix evaluated in equation (4) is further decomposed into its metallic contribution Σ , and Σ^0 the contribution due to direct interaction among the N coupled dipoles.

$$\Sigma_{jk}^{total}(\omega) = \Sigma_{jk}^0(\omega) + \Sigma_{jk}(\omega) \quad (7)$$

These are given by a corresponding decomposition of the Green tensors \mathbf{G} coupling two emitters in the presence of the metal nanoparticle.

$$\mathbf{G}(\mathbf{r}_k, \mathbf{r}_j; \omega) = \mathbf{G}_0(\mathbf{r}_k, \mathbf{r}_j; \omega) - \hat{G}_{jp} \hat{G}_{pq}^{-1} \hat{G}_{qk} \quad (8)$$

where the metal particle is in turn decomposed finely into many (552) dipole grains p, q to include the effect of its higher order modes. This numerical approach allows us to include retarded interactions in a system of dimensions comparable to the wavelength of emission. The size of the grain is determined by the wavelength of emission and material properties of the nanoparticle, and the number of such polarizable oscillators m arranged in a hexagonal close packed form can be increased as required for any given accuracy. The global matrices containing the Green dyads as 3×3 blocks are given by

$$\hat{G}_{pq}(3p \rightarrow 3p + 2, 3q \rightarrow 3q + 2) = \mathbf{G}_0(\mathbf{r}_p, \mathbf{r}_q; \omega) \quad (9)$$

$$\hat{G}_{jp}(1 \rightarrow 3, 3p \rightarrow 3p + 2) = \mathbf{G}_0(\mathbf{r}_j, \mathbf{r}_p; \omega) \quad (10)$$

$$\hat{G}_{qk}(3q \rightarrow 3q + 2, 1 \rightarrow 3) = \mathbf{G}_0(\mathbf{r}_q, \mathbf{r}_k; \omega) \quad (11)$$

The self-interaction of these polarizable grains in the metal particle $\mathbf{G}_0(\mathbf{r}_p, \mathbf{r}_p; \omega)$ are given by inverse of their polarizability α , which can be determined from its size and the dispersive permittivity of the material, using the Clausius-Mosotti relation [42] and its extensions to include the lattice dispersion [43]. \mathbf{G}_0 is calculated using the solutions of point source in a homogeneous background:

$$\nabla \times \nabla \times \mathbf{G}_0(\mathbf{r}, \mathbf{r}_j; \omega) - k^2 \mathbf{G}_0(\mathbf{r}, \mathbf{r}_j; \omega) = \mathbf{I} \delta(\mathbf{r} - \mathbf{r}_j) \quad (12)$$

where \mathbf{I} is a unit dyad, the wave number $k = \sqrt{\epsilon} \frac{\omega}{c}$, and $\delta(\mathbf{r} - \mathbf{r}_j)$ represents the point source. This gives us the dyadics for direct interaction among the point-dipoles:

$$\mathbf{G}_0(\mathbf{r}_i, \mathbf{r}_j; \omega) = (\mathbf{I} + \frac{\nabla \nabla}{k^2}) g(|\mathbf{r}_i - \mathbf{r}_j|) \quad (13)$$

where $g(r) = \frac{e^{ikr}}{4\pi r}$. The total decay rate Γ in the metal is decomposed into its radiative (Γ^r) and non-radiative (Γ^{nr}) by a factorization of \hat{G}_{pq} using real and imaginary parts of polarizability of dipole granules, which represent the metal nanoparticle in this volume integral approach [35]. The eigenstates of the coupled many emitter-metal system are calculated using:

$$\Sigma^{total}|J\rangle = \Delta_J - i \frac{\Gamma_J}{2} |J\rangle \quad (14)$$

Specifically, eigenvectors J represent one of N collective modes of emission here. The imaginary part of an eigenvalue of Σ^{total} represents decay rate of the mode while the real part of the eigenvalue represents the energy shift. The energy shifts ΔE_J of a collective mode can also be evaluated.

$$\hbar \Omega_J = 2\Delta E_J = 2\hbar |\Delta_J| \quad (15)$$

Note that $|J\rangle$ is not an eigenstate of Σ that represents only the metallic contribution. We evaluate contributions of the metal to the energy shifts and decay rates of a mode using an entry-wise decomposition of Σ_{jk} for all ' j ' and ' k ', into $\Delta_{jk} - i\Gamma_{jk}/2$ and corresponding expectations $\langle J|\Delta|J\rangle$ and $\langle J|\Gamma|J\rangle$. The strength of coupling between emitters through the metal is given by $K_{jk} = 2|\Delta_{jk}|/\Gamma_{jk}$ and its expectation $\langle J|K|J\rangle$ averaged over $|J\rangle$ represents the significance of non-classical metallic paths of the photon for the system (Figure 2b). Similarly, the one-loop correction to the decay rates is given by entries of a matrix Γ_{jk}^{leak} calculated as:

$$\Gamma_{jk}^{leak} = e^{-\frac{\Gamma_{jk}}{2\Delta_{jk}}} \cdot \Gamma_{jk}^{nr(1)} \quad (16)$$

Here the superscript (1) refers to the contribution of the dipole mode of the metal nanoparticles. The mode-wise Γ_{leak} is calculated by the expectation $\langle J|\Gamma_{leak}|J\rangle$. The one-loop correction to determine the effective decay rates of a collective mode remain as given in equation

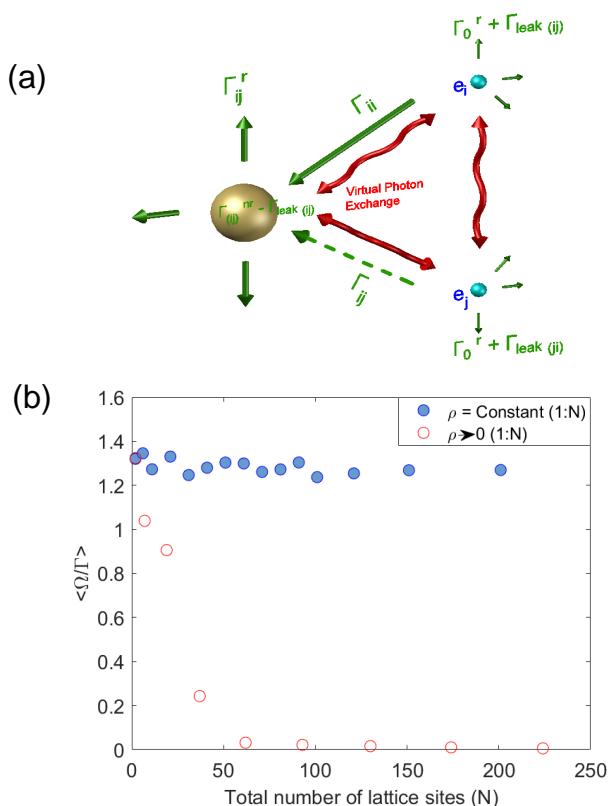


FIG. 2. (a) The one-loop corrections extended to multiple emitters i and j ; it includes non-classical paths (Rabi oscillations) among emitters, and also between an emitter and the metal nanoparticle. (b) The expected ratio of Rabi frequency and decay rate in the metal (coupling strength) due to a Markovian interaction with the metal.

(2). The quantum efficiency of a mode and the expected quantum efficiency are given by:

$$Q_J = \frac{\Gamma_{eff}^r}{\Gamma_{eff}^r + \Gamma_{eff}^{nr}} \quad Q = \frac{1}{N} \sum_{J=1}^N Q_J \quad (17)$$

III. RESULTS

For our analysis of results, let ρ be the average measure of the coupling of emitters with metal nanoparticles, and it is defined as:

$$\rho = \frac{n_{nc} + n_c}{l_{nc} + l_c + n_{nc} + n_c} \quad (18)$$

where n represents the number of paths of the photon involving the metal and l represents paths involving only the emitters; subscripts c and nc indicate classical and non-classical paths respectively. ρ_{nc} is a measure of the paths due to Rabi oscillations between the emitters and metal nanoparticles, while ρ_c is a measure of its weak coupling. They include only n_{nc} or n_c respectively in

the numerator of equation (18). In the weak coupling regime $\rho_{nc} = 0$, while in strong coupling regime both ρ_c and ρ_{nc} are non-zero. We investigate two conditions in each of the two cases. Case I: $\rho_{nc} = 0$; (a) $\rho = \text{constant}$ and (b) $\rho \rightarrow 0$. Case II: $\rho_{nc} \neq 0$; (a) $\rho = \text{constant}$ and (b) $\rho \rightarrow 0$. In both cases I and II, $\rho = \text{constant}$ represents an increase in the number of emitters within a constant area, while $\rho \rightarrow 0$ represents a case of increase in the number of emitters with a constant area density. A description of the geometries used in these cases is given below.

A. Model description

Here we explain the details of geometries corresponding to $\rho = \text{constant}$ and $\rho \rightarrow 0$ used for simulations in figures 2 and 4 of the paper. The emission wavelength of emitters is 560 nm in free-space and the refractive index of surrounding medium is 1.5. $Q_o = 0.33$ was assumed, and gold nanoparticles of diameter 3.8 nm are coupled to many dipole emitters. Each data point in the figures involve a number of simulations of many random configuration of polarizations and permuted positions, numbering greater than N until the relative variation in the expectation of the computed value is small.

1. Constant area : $\rho = \text{constant}$

Here we consider $N - 1$ dipole emitters around a metal nanoparticle of diameter 3.8 nm at an average distance of $h=7.6$ nm from the surface of the nanoparticle as shown in Figure 3. The point dipole emitters are uniformly distributed in a fixed area of shell of 2 nm. The decay rates are computed with increasing number of emitters in the shell to observe the effect of non-classical paths with metal nanoparticle. The quantum efficiency is roughly constant with the increase of number of emitters as shown by constant quenching in Figure 4a when limited to the classical paths through the metal particle, and constant enhancement in 4b due to inclusion of the non-classical paths through the metal nanoparticle. Note that paths l that include only emitters, and classical paths involving metal n_c increase as a factorial of N . But so does the non-classical paths n_{nc} due to Rabi oscillations between the metal and emitters, which is relevant for case II. The latter is possible as the stronger coupling of all emitters with the metal is ensured in this geometry. This ensures that the fraction of metallic paths $\rho \approx \text{constant}$.

2. Constant area density : $\rho \rightarrow 0$

Here we consider $N - 1$ dipole emitters around a metal nanoparticle of diameter 3.8 nm, where distances among emitters are fixed so that number of emitters per unit area i.e. area density is constant (see Figure 3). The

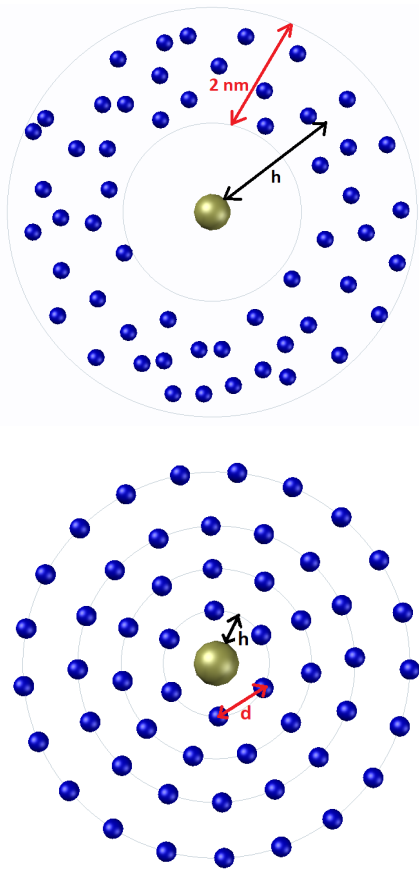


FIG. 3. The larger (golden) sphere is a gold nanoparticle of radius 1.9 nm. The smaller (blue) spheres represents dipole emitters where h is distance between nearest emitters and the nanoparticle. Top: Emitters distributed with a constant area: $\rho \approx \text{constant}$ with increase of sites. Bottom: Emitters distributed with a constant area density: $\rho \rightarrow 0$ with increase of sites.

first emitter is placed at a distance of $h=7.6$ nm from the surface of the metal nanoparticle and then additional emitters are placed on lattice sites which are at $d \approx 9.5$ nm apart from each other. The lattice sites are located in concentric circles around metal nanoparticle and distance between them is chosen so that first circle around metal contains exactly 6 emitters which may represent a hexagonal lattice. Note that the non-classical paths l involving only emitters increases as a factorial of N , while the non-classical paths n_{nc} through Rabi oscillation with metal marginally increases with N up to a constant, beyond which emitters are not coupled strongly enough to the metal. The classical paths n_c due to a weak coupling increase as a factorial of N initially, but as the couplings reduce further it converges to a constant when the farther emitters are not sufficiently coupled to the metal particle. This results in the fraction of metallic paths $\rho \rightarrow 0$ as N increases.

But both ρ and ρ_{nc} increase when some of the emitters are randomly replaced by metal nanoparticles on same

lattice sites so that overall metal to lattice sites ratio is 1:6. The green squares in Figure 4 show this qualitative behaviour and these simulations include 224 lattice sites out of which 37 are metal nanoparticles. Note that we used dipole metal nanoparticles to model this special case because of computational complexity of the multipole nanoparticle, and this underestimates the quenching and marginally overestimates the efficiency of emission.

B. Discussion

In case I, the Rabi oscillations (non-classical paths) between the emitters are accounted in the superpositions but the Rabi oscillations with the metal particle are ignored. This leads to a predicted quenching of emission and a reduction in quantum efficiency as shown in Figure 4a. The evaluated strengths of coupling with the metal particle shown in Figure 2 indicate the possible breakdown of this approximation. This quenching is constant when the number of emitters increase in a constant area as $\rho = \rho_c$ is constant. When the system expands with a constant area density of emitters, this quenching due to the metal particle decreases as does the fraction of paths of emitted photons through the dissipative metal particle. When some of the emitters in the model are replaced by metal particles (to reach a ratio of 1:6 for number of metal particles and emitters), quenching in the Markovian approximation is regained even when this system has now an extended area with many coupled emitters and metal particles.

In case II, the Rabi oscillations among emitters as well as with the metal particle, are included. The non-classical paths between emitters and the metal nanoparticle leads to enhancements in the quantum efficiency (Figure 4b). This enhancement is constant as the number of emitters increase in a constant area, as both ρ_c and ρ_{nc} remain roughly constant. When the system is expanded with a constant area density of emitters $\rho_{nc} \rightarrow 0$ due to weaker couplings, as does ρ_c . This results in a reduction of Rabi oscillations through the metal particle, and the lost enhancement is only regained when some of the emitters are replaced by metal nanoparticles fixing a ratio of 1:6 for the metal nanoparticles and the emitters.

The evaluations for the two geometries, and the two approximations i.e. the Markovian and its one-loop correction, confirm that the one-loop correction presents physically meaningful predictions when the number of interacting emitters are many, and also with multiple metal particles. It should be noted that when the coupling of the emitter becomes stronger at small relative separations with the particle, this correction diverges and a full non-Markovian model of interaction becomes indispensable [26]. From the above two cases studied, we can infer that the coherence of non-classical paths among many strongly coupled emitters and metal nanoparticles is sustained independent of the number of emitters and metal particles. This effect diminishes only when a large frac-

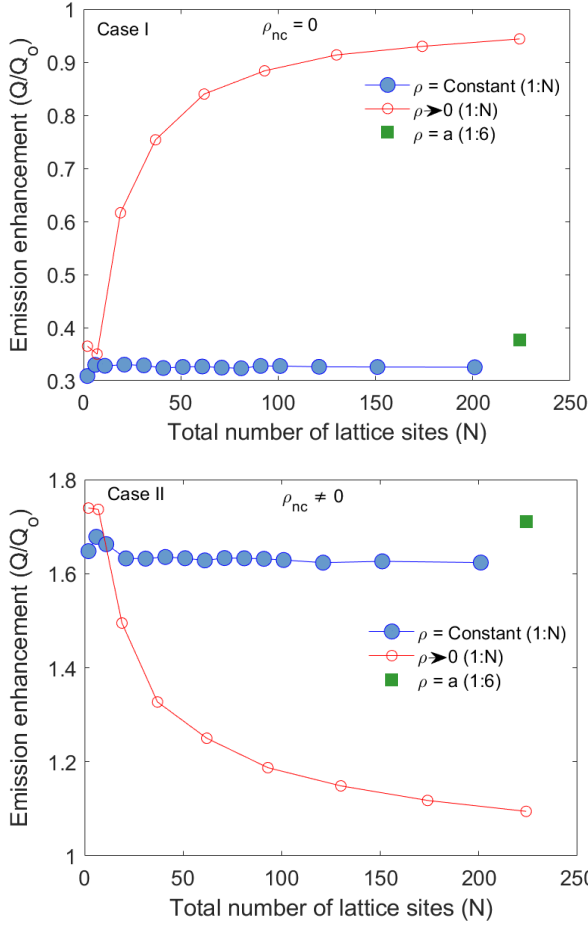


FIG. 4. Modified emission due to gold nanoparticles 1.9 nm in radii, free-space emission wavelength $\lambda = 560$ nm and $Q_0 = 1/3$ (I) quenching when only classical paths of the metal are included (II) enhancements when non-classical paths of metal are also included.

tion of emitters are weakly coupled to the metal nanoparticle i.e. when separations between the emitters and a lone metal particle increase. Considering the lower dissipative loss of these very small metal particles they are expected to be much more effective in enhancement of spontaneous emission, compared to the larger metal particles required in the weak-coupling regime. Further, the emerging coherence and dynamics of emission in such materials can be exploited for applications other than light generation [44].

ACKNOWLEDGMENTS

K.J. and M.V. thank the department of Computational & Data Sciences, Indian Institute of Science for its generous support.

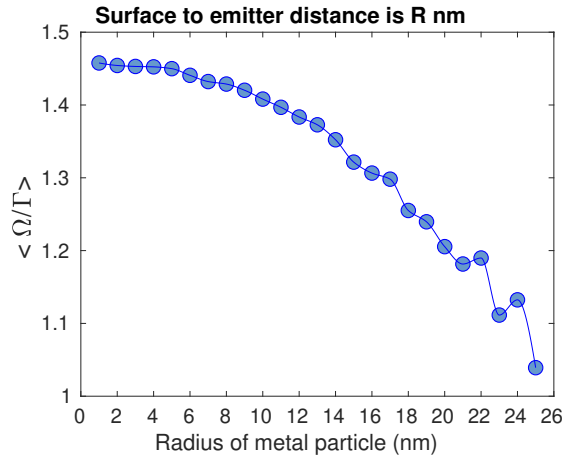


FIG. A2. Coupling strengths of a single emitter and a gold nanoparticle as determined by the Markovian model, which can be used for one-loop corrections.

Appendix A: Coupling strengths and size of gold nanoparticles

A larger factor $e^{-\Gamma/\Omega}$, determines the degree of divergence of observations from the predictions of the Markovian (weak-coupling) approximation of the emitter and the metal nanoparticle. Variation of this exponent in a logarithmic scale are plotted below in Figures A1 and A2 for a fixed small distance of 3 nm and for a 'relative' distance fixed as the radius 'R' of metal particle. All the above cases represent gold nanoparticles with a surrounding medium of refractive index 1.5, and at a free-space wavelength of 560 nm.

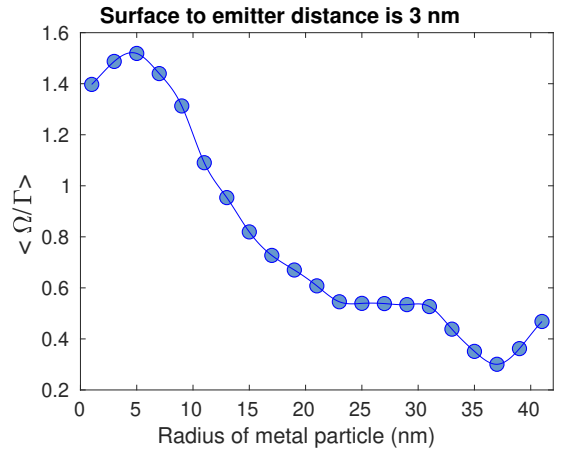


FIG. A1. Coupling strengths of a single emitter and a gold nanoparticle as determined by the Markovian model, which can be used for one-loop corrections.

-
- [1] Y. Zhu, D. J. Gauthier, S. E. Morin, Q. Wu, H. J. Carmichael, and T. W. Mossberg, *Phys. Rev. Lett.* **64**, 2499 (1990).
- [2] F. Bernardot, P. Nussenzeveig, M. Brune, J. M. Raimond, and S. Haroche, *Europhys. Lett.* **17**, 33 (1992).
- [3] A. Boca, R. Miller, K. M. Birnbaum, A. D. Boozer, J. McKeever, and H. J. Kimble, *Phys. Rev. Lett.* **93**, 233603 (2004).
- [4] T. Yoshie, A. Scherer, J. Hendrickson, G. Khitrova, H. M. Gibbs, G. Rupper, C. Ell, O. B. Shchekin, and D. G. Deppe, *Nature* **432**, 200 (2004).
- [5] J. Bellessa, C. Bonnand, J. C. Plenet, and J. Mugnier, *Phys. Rev. Lett.* **93**, 036404 (2004).
- [6] G. Zengin, M. Wersäll, T. J. Nilsson, S. Antosiewicz, M. Kall, and T. Shegai, *Phys. Rev. Lett.* **114**, 157401 (2015).
- [7] A. E. Schlather, N. Large, A. S. Urban, P. Nordlander, and N. J. Halas, *Nano Lett.* **13**, 3281 (2013).
- [8] N. Vats, S. John, and K. Busch, *Phys. Rev. A* **65**, 043808 (2002).
- [9] D. E. Chang, A. S. Sørensen, P. R. Hemmer, and M. D. Lukin, *Phys. Rev. B* **76**, 035420 (2007).
- [10] C. Van Vlack, P. T. Kristensen, and S. Hughes, *Phys. Rev. B* **85**, 075303 (2012).
- [11] A. Delga, J. Feist, J. Bravo-Abad, and F. J. Garcia-Vidal, *Phys. Rev. Lett.* **112**, 253601 (2014).
- [12] M. Pelton, S. D. Storm, and H. Leng, *Nanoscale* **11**, 14540 (2019).
- [13] K. Jain and M. Venkatapathi, *Phys. Rev. Appl.* **11**, 054002 (2019).
- [14] R. Dutta, K. Jain, M. Venkatapathi, and J. K. Basu, *Phys. Rev. B* **100**, 155413 (2019).
- [15] G. C. Schatz, M. A. Young, and R. P. Van Duyne, in *Surface-enhanced Raman scattering* (Springer, 2006) pp. 19–45.
- [16] M. Moskovits, *Phys. Chem. Chem. Phys.* **15**, 5301 (2013).
- [17] K. Kneipp, *J. Phys. Chem. C* **120**, 21076 (2016).
- [18] S. Heeg, N. S. Mueller, S. Wasserroth, P. Kusch, and S. Reich, *J. Raman Spectrosc.* **52**, 310 (2021).
- [19] M. Haridas and J. K. Basu, *Nanotechnol.* **21**, 415202 (2010).
- [20] M. Haridas, J. K. Basu, D. J. Gosztola, and G. P. Wiederrecht, *Appl. Phys. Lett.* **97**, 189 (2010).
- [21] K. A. Kang, J. Wang, J. B. Jasinski, and S. Achilefu, *J. Nanobiotechnol.* **9**, 16 (2011).
- [22] M. Haridas, J. K. Basu, A. K. Tiwari, and M. Venkatapathi, *J. Appl. Phys.* **114**, 064305 (2013).
- [23] A. Gonzalez-Tudela, F. J. Rodríguez, L. Quiroga, and C. Tejedor, *Phys. Rev. B* **82**, 115334 (2010).
- [24] K. H. Madsen, S. Ates, T. Lund-Hansen, A. Löffler, S. Reitzenstein, A. Forchel, and P. Lodahl, *Phys. Rev. Lett.* **106**, 233601 (2011).
- [25] G. Agarwal, *Quantum Optics* (Cambridge University Press, 2013).
- [26] K. Jain and M. Venkatapathi, manuscript under review, supplemental material for referees (2021).
- [27] M. Macovei, J. Evers, G.-x. Li, and C. H. Keitel, *Phys. Rev. Lett.* **98**, 043602 (2007).
- [28] V. Shatokhin, C. Müller, and A. Buchleitner, *Phys. Rev. Lett.* **94**, 043603 (2005).
- [29] A. Safari, R. Fickler, E. Giese, O. S. Magaña-Loaiza, R. W. Boyd, and I. De Leon, *Phys. Rev. Lett.* **122**, 133601 (2019).
- [30] M. Venkatapathi, *J. Quant. Spectros. Radiat. Transfer* **113**, 1705 (2012).
- [31] A. A. Svidzinsky, J. Chang, and M. O. Scully, *Phys. Rev. A* **81**, 053821 (2010).
- [32] R. Wiegner, J. Von Zanthier, and G. S. Agarwal, *Phys. Rev. A* **84**, 023805 (2011).
- [33] L. Jin, J. Evers, and M. Macovei, *Phys. Rev. A* **84**, 043812 (2011).
- [34] V. N. Pustovit and T. V. Shahbazyan, *Phys. Rev. B* **82**, 075429 (2010).
- [35] M. Venkatapathi, *J. Opt. Soc. Am. B* **31**, 3153 (2014).
- [36] J. Tignon, P. Voisin, C. Delalande, M. Voos, R. Houdré, U. Oesterle, and R. P. Stanley, *Phys. Rev. Lett.* **74**, 3967 (1995).
- [37] V. Debierre, T. Durt, A. Nicolet, and F. Zolla, *Phys. Lett. A* **379**, 2577 (2015).
- [38] A. Schülzgen, R. Binder, M. Donovan, M. Lindberg, K. Wundke, H. Gibbs, G. Khitrova, and N. Peyghambarian, *Phys. Rev. Lett.* **82**, 2346 (1999).
- [39] G. S. Agarwal, *J. Opt. Soc. Am. B* **2**, 480 (1985).
- [40] H. Kamada, H. Gotoh, J. Temmyo, T. Takagahara, and H. Ando, *Phys. Rev. Lett.* **87**, 246401 (2001).
- [41] F. Alpegiani, S. D'Agostino, and L. C. Andreani, *Phys. Rev. B* **86**, 035421 (2012).
- [42] E. M. Purcell and C. R. Pennypacker, *Astrophys. J.* **186**, 705 (1973).
- [43] B. T. Draine and P. J. Flatau, *J. Opt. Soc. Am. A* **11**, 1491 (1994).
- [44] M. Otten, R. A. Shah, N. F. Scherer, M. Min, M. Pelton, and S. K. Gray, *Phys. Rev. B* **92**, 125432 (2015).